Chondroitin Sulfate Prevents Peritoneal Fibrosis in Mice by Suppressing NF-κB Activation

Shinichi Abe[1, 2], Yoko Obata[1, 3], Satoru Oka[1], Takehiko Koji[4], Tomoya Nishino[1], and Koichi Izumikawa[2]

[1] Department of Nephrology, Nagasaki University Hospital

[2] Department of infectious disease, Unit of molecular Microbiology and Immunology, Nagasaki University Graduate School of Biomedical Sciences

[3]Medical Education Development Center, Nagasaki University Hospital

[4]Department of Histology and Cell Biology, Unit of Basic Medical Science, Nagasaki University Graduate School of Biomedical Sciences

Corresponding author: Yoko Obata, M.D., Ph.D.

Department of Nephrology, Nagasaki University Hospital

1-7-1 Sakamoto, Nagasaki City, Japan

Tel: +81-95-819-7273, Fax: +81-95-849-7285

E-mail: yobata@nagasaki-u.ac.jp

Key words: chondroitin sulfate, peritoneal fibrosis, NF-κB, mitogen-activated protein kinase, chlorhexidine gluconate

ABSTRACT

Long-term peritoneal dialysis causes peritoneal fibrosis, and previous reports suggest that inflammation plays a critical role in peritoneal fibrosis. Chondroitin sulfate (CS) suppresses the inflammatory response by preventing activation of nuclear factor (NF)-κB. We examined the effect of CS on the peritoneal fibrosis induced by chlorhexidine gluconate (CG) in mice. CS or water was administered daily. We divided mice into four groups: administered vehicle and water (control); administered vehicle and CS (CS); administered CG and water (CG); and administered CG and CS (CG + CS). Morphologic changes were assessed by Masson's trichrome staining. Inflammation- and fibrosis-associated factors were assessed by immunohistochemistry. Activation of NF-κB was examined by southwestern histochemistry (SWH). CS administration suppressed the progression of submesothelial thickening. The numbers of inflammation- and fibrosis-associated factors -positive cells were significantly decreased in the CG + CS group, compared to the CG group. Based on SWH, the CG + CS group contained significantly fewer NF-κB-activated cells than the CG group. Our results indicate that CS suppresses peritoneal fibrosis via suppression of NF-κB activation. These results suggest that CS has therapeutic potential for peritoneal fibrosis.

INTRODUCTION

Peritoneal dialysis (PD) is a beneficial therapy for end-stage renal disease. However, long-term PD therapy leads to histopathological changes in the peritoneum, such as peritoneal fibrosis, increased submesothelial collagen deposition, and loss of mesothelial cells [1, 2]. In particular, submesothelial collagen deposition was reported to be correlated with reduced ultrafiltration capacity, which accounted for about 20% of patient withdrawals from PD [3, 4]. Moreover, some patients with peritoneal fibrosis developed encapsulating peritoneal sclerosis (EPS), which is one of the most critical complications of PD and is associated with high mortality. However, the mechanism of peritoneal fibrosis in PD patients remains poorly understood and no effective therapy is available. Previous reports suggest that inflammation plays a crucial role in peritoneal fibrosis [2, 5]. Therefore, an unexplored avenue for successful peritoneal fibrosis treatment is attenuating peritoneal inflammation.

Nuclear factor (NF)-κB is a transcription factor that controls the transcription of several genes involved in immune and inflammatory responses, cell growth, and adhesion, and is ubiquitously expressed in most cell types [6, 7]. NF-κB mediates the production of chemokines and cytokines, such as monocyte chemoattractant protein-1 (MCP-1) or interleukin-1β (IL-1β) [8, 9]. MCP-1 plays an important role in the

initiation and progression of inflammatory processes that involve macrophage infiltration in peritoneal fibrosis [10]. Increased NF-κB expression was observed in infiltrating cells of the submesothelial compact zone and increased NF-κB activation was also observed in the peritoneum of PD-treated patients [10]. In fact, inhibition of NF-κB activation suppressed peritoneal fibrosis [11, 12].

Chondroitin sulfate (CS) is an unbranched, polydisperse, complex glycosaminoglycan (GAG). It is present in the extracellular matrix surrounding cells, especially in the cartilage, skin, blood vessels, ligaments, and tendons. Previous reports suggest that CS has anti-inflammatory activity via suppression of NF-κB activation [13, 14]. CS suppresses NF-κB activation by inhibiting the phosphorylation of extracellular signal-regulated kinase 1/2 (ERK1/2) and p38 mitogen-activated protein kinase (p38MAPK), which both induce the nuclear translocation of NF-κB via Ikappa B (IκB) degradation [13, 14, 15]. Studies using a mouse type II collagen-induced arthritis model [16], a rat dextran sulfate sodium-induced colitis model [17], and a rabbit atherosclerotic model [18] have demonstrated that CS attenuates the state of each disease via suppression of inflammation. In this regard, CS may ameliorate peritoneal fibrosis via suppression of peritoneal inflammation. Therefore, we examined the effect of CS on peritoneal fibrosis in a mouse chlorhexidine gluconate (CG)-induced

peritoneal fibrosis model.

MATERIALS AND METHODS

ANIMAL MODELS

The animals used in this study were male ICR mice (10 weeks of age, weighing approximately 40 g; Japan SLC Inc., Shizuoka, Japan). The animals had free access to laboratory chow and tap water and were housed in a light- and temperature-controlled room at the Laboratory Animal Center of Nagasaki University School. The experimental protocol was inspected by the Animal Care and Use Committee of Nagasaki University School and approved by the President of Nagasaki University School (approval number: 1004050846).

EXPERIMENTAL PROCEDURES

Peritoneal fibrosis was induced by intraperitoneal injection of 0.1% CG in 15% ethanol dissolved in saline, as described previously [19]. Mice received injections of 0.1% CG in 15% ethanol dissolved in saline or 15% ethanol dissolved in saline only, at a dose of 0.2 mL/body into the peritoneal cavity, on alternate days for 3 weeks. CS (chondroitin-4-sulfate sodium salt from bovine trachea; C 9819; Sigma, St. Louis, USA) dissolved in water was administered daily via an oral gastric tube at a dose of 500 mg/kg. Mice were assigned to one of four groups: (1) the control group, which included

mice administered 15% ethanol dissolved in saline intraperitoneally and water orally (*n* = 10); (2) the CS group, which included mice administered 15% ethanol dissolved in saline intraperitoneally and CS orally (*n* = 10); (3) the CG group, which included mice administered CG intraperitoneally and water orally (*n* = 10); and (4) the CG + CS group, which included mice administered CG intraperitoneally and CS orally (*n* = 10).

Mice were sacrificed at day 21 after the first CG injection, and peritoneal tissues were carefully dissected. To avoid direct damage to the peritoneum due to repeated injections, CG was injected into the lower part of the peritoneum, preserving the upper portion of the parietal peritoneum for examination. Immediately after sampling, the tissues were fixed with 4% paraformaldehyde in phosphate-buffered saline (PBS; pH 7.4) and then embedded in paraffin. For morphological examination of the peritoneum, 4-μm thick, paraffin-embedded tissues were stained with Masson's trichrome staining.

IMMUNOHISTOCHEMISTRY

Paraffin-embedded tissue sections were stained immunohistochemically using an indirect method. The following antibodies were used for immunohistochemistry: (1) rabbit anti-phosphorylated p38MAPK monoclonal antibody diluted 1:10 (4631: Cell Signaling Technology, Massachusetts, USA); (2) mouse anti-phosphorylated ERK1/2

monoclonal antibody diluted 1:10 (M 8159; Sigma); (3) goat anti-mouse MCP-1 antibody diluted 1:100 (sc-1784; Santa Cruz Biotechnology, Santa Cruz, CA, USA); (4) rat anti-F4/80 antibody, diluted 1:50 (MCA497; Serotec, Oxford, UK), used as a marker of mouse macrophages; (5) rabbit anti-human phosphorylated Smad2/3 antibody diluted 1:50 (sc-11769-R; Santa Cruz Biotechnology); (6) rabbit anti-IL-1β antibody, diluted 1:50 (sc-7884; Santa Cruz Biotechnology); (7) rabbit anti- IκBα antibody, diluted 1:50 (ab32518; Abcam, Cambridge, UK); and (8) Rat anti-CD86 antibody, diluted 1:50 (558703, BD Pharmingen, NJ, USA), used as a marker of M1 macrophage. After deparaffinization, the sections were treated with 0.3% H_2O_2 in methanol for 20 min to inactivate endogenous peroxidase. For the immunohistochemical analysis of phosphorylated Smad2/3, IL-1β, IκBα, and CD86, the sections were treated in a microwave oven (MI-77; Azumaya, Tokyo, Japan) at 95°C in 10 mM citrate buffer (pH 6.0), 5 min for phosphorylated Smad2/3, 15 min for others before H_2O_2 treatment for antigen retrieval. For the immunohistochemical analysis of phosphorylated p38MAPK, phosphorylated ERK1/2, F4/80 and MCP-1, the sections were treated with proteinase K (P2308; Sigma) for 15 min at 37°C before H_2O_2 treatment for antigen retrieval. The sections were incubated for 30 min with a blocking solution (5% normal goat serum, 5% fetal calf serum, 5% bovine serum albumin (BSA), and 20% normal swine serum in

PBS) at room temperature. The sections were then exposed to the primary antibody, which was diluted in blocking buffer. For phosphorylated p38MAPK, MCP-1, IL-1β, IκBα, CD86, and phosphorylated Smad2/3 staining, sections were stained with an avidin–biotin complex using a Vectastain Elite ABC kit (Vector Laboratories, Burlingame, CA, USA) after reaction with the primary antibody. For phosphorylated ERK1/2, the sections were exposed to a complex of anti-phosphorylated ERK1/2 antibody and horseradish peroxidase (HRP)-conjugated rabbit anti-mouse immunoglobulin antibody (P0161; Dako, Glostrup, Denmark) diluted 1:10 for 30 min at room temperature. Then, sections were incubated with EnVision+ System-HRP Labelled Polymer Anti-Rabbit (K4002, Dako) for 30 min at room temperature. For F4/80, after incubation with primary antibodies overnight at 4°C, the sections were incubated with HRP-conjugated rabbit anti-rat immunoglobulin antibody (P0450; Dako) and HRP-conjugated swine anti-rabbit immunoglobulin antibody (P0399; Dako), diluted 1:50, for 30 min at room temperature. The reaction sites were visualized by treating the sections with H_2O_2 and 3,3-diaminobenzidine tetrahydrochloride (DAB). Finally, the sections were counterstained with methyl green and mounted. For all specimens, negative controls were prepared using normal IgG instead of the primary antibody.

IMMUNOFLUORESCENCE STAINING

Mouse anti-α-smooth muscle actin (α-SMA) antibody, diluted 1:100 (A2547; Sigma), was used an immunofluorescent marker for myofibroblasts. After deparaffinization, the sections were autoclaved at 120°C for 10 min in 10 mM citrate buffer (pH 6.0). The sections were incubated for 1 h with a blocking solution consisting of 500 μg/mL normal goat IgG and 1% BSA in PBS at room temperature. The sections were then incubated with the primary antibodies, which were diluted in the same blocking solution. The sections were incubated with Alexa Fluor 488-labeled goat anti-mouse IgG (A11078; Invitrogen, Paisley, UK) for 1 h, stained with 4,6-diamidino-2-phenylindole (DAPI) for 1 min, and then mounted. Images of the sections were acquired using a confocal laser scanning microscope (LSM 5 PASCAL; Carl Zeiss Co., Ltd., Obekochen, Germany). Normal goat IgG was used as a negative control.

QUANTIFICATION OF PROTEINS BY ELISA

Protein concentration in PD effluent was evaluated using an enzyme-linked immunosorbent assay (ELISA) for MCP-1 (MJE00; R&D Systems, Minneapolis MN, USA). PD effluent was collected with following method; after anesthesia with mixed anesthetic agent (0.75 mg/kg of medetomidine, 4.0 mg/kg of midazolam, and 5.0 mg/kg

of butorphano), a silicon catheter was inserted into the peritoneal cavity and 10.0 ml of a standard dialysate (Dianeal; Baxter International Inc., Deerfield, IL, USA) containing 2.5% glucose was instilled, and dialysate samples were obtained at 60 min after administration of dialysate. Optical density was measured using a microplate reader (MULTISKAN FC; Thermo Scientific, Kanagawa, Japan).

SOUTHWESTERN HISTOCHEMISTRY FOR NF-κB

The single-stranded (ss) oligo-DNAs 5´-GATCGAGGGGGACTTTCCCTAGC-3´ and 5´-GCTAGGGAAAGTCCCCCTCGATC-3´ were synthesized to recognize the NF-κB binding site consensus sequence [20]. Double-stranded (ds) oligo-DNA was 3´-labeled with digoxigenin (DIG). The synthesized ss oligo-DNAs were purchased from BEX (Tokyo, Japan). For annealing of complementary ss oligo-DNAs to ds oligo-DNA, the ss oligo-DNAs were dissolved in 10 mM of Tris-HCl buffer (pH 7.4), denatured for 10 min at 100°C, and gradually cooled to room temperature.

Southwestern histochemistry (SWH) was performed as described previously [21-23]. Briefly, deparaffinized sections (4 μm thick) were incubated in citrate buffer (pH 6.0) in a microwave oven at 95°C for 15 min. The sections were then washed in PBS and immersed in a pre-incubation buffer containing 5% nonfat milk dissolved in

500 mM NaCl, 1 mM EDTA, and 10 mM Tris-HCl (pH 7.4) for 1 h. The sections were then incubated with the DNA-oligo probes (2 μg/mL) in pre-incubation buffer overnight. The sections were washed twice with pre-incubation buffer and four times with 0.075% Brij in PBS. Then, the sections were incubated in a blocking buffer containing 5% BSA, 500 μg/mL of normal sheep IgG, 100 μg/mL of yeast transfer RNA, and 100 μg/mL of salmon sperm DNA in PBS for 1 h. To visualize hybridized DNA-oligo probes, the sections were immunohistochemically stained with HRP-conjugated anti-DIG sheep antibody (1207733; Roche, Mannheim, Germany), diluted 1:100 in blocking buffer, for 2 h. After four washes with 0.075% Brij in PBS, we visualized the HRP sites in a chromogen solution containing 0.5 mg/mL DAB, 0.01% H_2O_2, 0.02% $Ni(NH_4)_2(SO_4)_2$, and 0.025% $COCl_2$. To evaluate the specificity of the probes for NF-κB, we also used mutated probes 5´-GATCGAGGAAGACTTTCCCTAGC-3´ and 5´-GCTAGGGAAAGRCTTCCTCGATC-3´ [19].

MORPHOMETRIC ANALYSIS

Digitized images and image analysis software were used to assess the extent of peritoneal thickening (Lumina vision; MITANI Corporation, Tokyo, Japan). The thicknesses of the submesothelial zone above the abdominal muscle in cross-sections of

the abdominal wall were measured. For each peritoneal sample, the number of phosphorylated p38MAPK-positive cells, phosphorylated ERK1/2-positive cells, α-SMA-positive myofibroblasts, phosphorylated Smad2/3–positive cells, MCP-1-expressing cells, IL-1β-positive cells, F4/80-positive macrophages, IκBα-positive cells, and NF-κB-positive cells were counted at × 200 magnification for five fields, each with a diameter of 1 mm. In the case of NF-κB detection by SWH, red color was given to the positive cells by an image analyzer (DAB System: Carl Zeiss, Gottingen, Germany). Positive cells were evaluated based on the staining density over the level of staining with the mutated probe.

STATISTICAL ANALYSIS

Data have been expressed as mean ± standard error mean (SEM). Differences among the four groups of mice (control, CG, CS, and CG + CS) were examined for statistical significance by using repeated measures analysis of variance (ANOVA) (Bonferroni/Dunn test). A p value of < 0.05 denoted statistical significance. All statistical analyses were performed using Stat View version 5.0 software (SAS Institute Inc., NC, USA).

RESULTS

MORPHOLOGICAL EXAMINATION FOLLOWING MASSON'S TRICHROME STAINING

In the control and CS groups, the peritoneal tissue consisted of a peritoneal mesothelial monolayer and sparse connective tissue below the layer (Fig. 1a, b and e). Compared to the control group, the peritoneal tissue of the CG group showed significant thickening of the submesothelial compact zone and the presence of numerous cells (Fig. 1c and e). The thickness of the submesothelial compact zone in the CG + CS group was significantly lesser than that of the CG group (Fig. 1c, d and e).

EXPRESSION OF PHOSPHORYLATED MAPK

We performed immunohistochemistry in the peritoneal tissues to detect phosphorylated p38MAPK and phosphorylated ERK1/2, both of are essential in the nuclear translocation of NF-κB. The CG group produced increased numbers of phosphorylated p38MAPK and phosphorylated ERK1/2-positive cells in the peritoneum (Fig. 2a, c, d and f) in comparison to the CG + CS group (Fig. 2b, c, e and f). In addition, we have performed immunohistochemistry for phosphorylated P38MAPK, phosphorylated ERK1/2, and F4/80 using continuous sections to investigate the involvement of macrophages in MAPK phosphorylation. The result suggested that almost all macrophages (Fig. 2h) were positive for phosphorylated P38MAPK (Fig. 2g)

and phosphorylated ERK1/2 (Fig. 2i), namely CS suppressed activation of ERK1/2 and P38MAPK in macrophages.

EXPRESSION OF ACTIVATED NF-κB

To investigate the expression levels of activated NF-κB in our model, we used SWH to detect activated transcription regulatory factors that bind to specific sequences of DNA [22, 23]. The number of NF-κB-activated cells in the submesothelial compact zone of the CG group was significantly higher than that of the control group (Fig. 3a and c). Compared to the CG group, the CG + CS group contained significantly fewer NF-κB-activated cells (Fig. 3a, b and c). To evaluate the specificity of our probes, we performed the same procedure using mutated probes. In this case, only weak nuclear staining for NF-κB was detected (Fig. 3d and e). Moreover, we performed the immunohistochemistry for IκBα to verify the inhibitory effect of CS for activation of NF-κB. As a result, the number of IκBα- positive cells in the CG+CS group was larger than that of the CG group (Fig. 3f and g). Thus, these findings suggested that CS suppressed the activation of NF-κB.

EXPRESSION OF MCP-1 and IL-1β

We investigated the effect of CS on MCP-1-expression, which strongly promotes macrophage infiltration. In the CG group, the number of MCP-1-expressing

cells was significantly higher than that of the control group (Fig. 4a and c). Compared to the CG group, the CG + CS group had significantly fewer MCP-1-expressing cells (Fig. 4a, b and c). We also evaluated the concentration of MCP-1 in PD effluent using ELISA. The concentration of MCP-1 was higher in the CG group than in the control group, but a significant reduction was observed for the CG + CS group (Fig. 4d). In addition, we investigated the expression of IL-1β as one of target genes of NF-κB by immunohistochemistry. In the CG group, IL-1β-positive cells were abundant in the thickened submesothelial compact zone (Fig. 4e and g), but the CG + CS group contained fewer IL-1β-positive cells (Fig. 4f and g).

INFILTRATION OF MACROPHAGE AND ITS PHENOTYPE

We stained sections with anti-F4/80 antibody to test for the presence of macrophages. For the CG group, we observed numerous macrophages in the thickened peritoneal tissues (Fig. 5a and c), but not in the CG + CS group, which contained relatively few macrophages (Fig. 5b and c). Furtheremore, we have performed immunohistochemistry for CD86, which is known as a marker for M1 macrophage, and F4/80 using continuous sections. We observed that almost all macrophages were positive for CD86 (Fig. 5d and e).

EXPRESSION OF PHOSPHORYLATED SMAD2/3 AND α-SMA

We examined TGF-β signaling by performing immunohistochemistry to detect phosphorylated Smad2/3, a mediator of TGF-β signaling that regulates fibrotic response. CG injection significantly increased the number of phosphorylated Smad2/3–positive cells in the thickened submesothelial compact zone in comparison to the control group (Fig .6a and c). Compared to the CG group, the CG + CS group had a markedly reduced number of the positive cells (Fig. 6a, b and c).

Next, we investigated α-SMA expression, which is an indicator of myofibroblasts, the main collagen producing cells. In the CG group, α-SMA-positive myofibroblasts were abundant in the thickened submesothelial compact zone (Fig. 6d and f), but the CG + CS group contained fewer α-SMA-positive myofibroblasts (Fig. 6d, e and f).

DISCUSSION

Here, we have demonstrated that CS prevented peritoneal fibrosis via suppression of NF-κB activation in mice. Moreover, treatment with CS reduced the number of MCP-1-positive cells, F4/80-positive macrophages which express mainly M1 phenotype, and α-SMA-positive myofibroblasts. These findings indicate that CS might be useful in preventing the progression of peritoneal fibrosis.

In the present study, we supposed that CS might suppress peritoneal fibrosis via inhibition of NF-κB activation. In fact, we demonstrated that CS reduced the number of

activated MAPK-positive, IκBα-positive and activated NF-κB-positive cells using immunohistochemistry and SWH, which are consistent with previous reports [16-18]. Moreover, CS attenuated MCP-1 expression, which is widely known to be one of chemokines regulated by NF-κB and important for infiltration of macrophages [9]. As a result, we observed that CS reduced the number of infiltrating macrophages in the submesothelial compact zone. Macrophages are a source of several fibrogenic genes, including TGF-β, which is known to play a pivotal role in the development of peritoneal fibrosis [24, 25]. Moreover, we showed that almost all macrophages express M1 phenotype. Since M1 macrophage is known to promote inflammation (26), our findings are compatible with previous literature. Thus, our results suggest that CS attenuates peritoneal fibrosis by suppressing macrophage infiltration and TGF-β/Smad signaling via suppression of NF-κB activation.

However, our approach has some limitations. First, there are some differences between CG-induced peritoneal fibrosis and human peritoneal fibrosis, although we used a murine CG-induced peritoneal fibrosis model in the present study. CG models induce a chemical irritant but the etiology of human EPS is more complicated. However, most of the histological changes in CG models are similar to peritoneal fibrosis in humans, namely, injection of CG results in progression of fibrosis and thickening of the

peritoneum similar to human peritoneal fibrosis. In addition, CG model is also reported to have elevated levels of proinflammatory cytokines, such as IL-1β and TNF-α [27]. Previous research has indicated that the production of proinflammatory cytokines is associated with peritoneal fibrosis [28]. Thus, we consider that CG model is a good model for peritoneal fibrosis in PD patients and useful to investigate the pathogenesis and therapy of peritoneal fibrosis. Second, the CS dose of 500 mg/kg per day used in this study, although consistent with previous work using animal models [16-18], is greater than the clinical dose used for humans with osteoarthritis, where CS is administered as SYSDOA (symptomatic slow acting drug for osteoarthritis) [29, 30]. The only reported side effects of CS administration in humans were abdominal pain and nausea [29, 30]. We observed no adverse events such as weight reduction, decreased liver or kidney function, or increased mortality on CS administration. Further studies are warranted to clarify whether, and at what dosage, CS can effectively reduce peritoneal fibrosis in PD patients.

CONCLUSION

We have shown that CS can suppress peritoneal fibrosis in a mouse CG-injected peritoneal fibrosis model via inhibition of NF-κB activation. Our results suggest that CS is a viable candidate as a novel therapeutic agent for peritoneal fibrosis.

ACKNOWLEDGEMENTS

This work was supported by grants from the Japanese Association of Dialysis Physicians (No. 25067). We would like to thank Ms. Ryoko Yamamoto and Ms. Ayako Matsuo for the excellent experimental assistance.

DISCLOSURES

All authors state that they have no conflicts of interest to declare.

REFERENCES

1) Williams JD, Craig KJ, Topley N, Von Ruhland C, Fallon M, Newman GR, Mackenzie RK, Williams GT (2002) Morphologic changes in the peritoneal membrane of patients with renal disease. J Am Soc Nephrol 13:470-9

2) Devuyst O, Margetts PJ, Topley N (2010) The pathophysiology of the peritoneal membrane. J Am Soc Nephrol 21:1077-85

3) Honda K, Hamada C, Nakayama M, Miyazaki M, Sherif AM, Harada T, Hirano H (2008) Impact of uremia, diabetes, and peritoneal dialysis itself on the pathogenesis of peritoneal sclerosis: a quantitative study of peritoneal membrane morphology. Clin J Am Soc Nephrol 3:720-8

4) Mizuno M, Ito Y, Tanaka A, Suzuki Y, Hiramatsu H, Watanabe M, Tsuruta Y. Matsuoka T, Ito I, Tamai H, Kasuga H, Shimizu H, Kurata H, Inaguma D, Hiramatsu T, Horie M, Naruse T, Maruyama S, Imai E, Yuzawa Y, Matsuo S (2011) Peritonitis is still an important factor for withdrawal from peritoneal dialysis therapy in the Tokai area of Japan. Clin Exp Nephrol 15:727-37

5) Yung S, Chan TM (2003) Preventing peritoneal fibrosis--insights from the laboratory. Perit Dial Int 23:S37-41

6) Baeuerle PA, Henkel T (1994) Function and activation of NF-κB in the immune system. Annu Rev Immunol 12:141-79

7) Schreck R, Rieber P, Baeuerle PA (1991) Reactive oxygen intermediates as apparently widely used messengers in the activation of the NF-κB transcription factor and HIV-1. EMBO J 10:2247-58

8) Ha H, Yu MR, Choi YJ, Kitamura M, Lee HB (2002) Role of high glucose-induced nuclear factor-kappaB activation in monocyte chemoattractant protein-1 expression by mesangial cells. J Am Soc Nephrol 13:894-902

9) Rovin BH, Dickerson JA, Tan LC, Hebert CA (1995) Activation of nuclear factor-kappa B correlates with MCP-1 expression by human mesangial cells. Kidney Int 48:1263-71

10) Kihm LP, Wibisono D, Muller-Krebs S, Pfisterer F, Morath C, Gross ML, Morcos M, Seregin Y, Bierhaus A, Nawroth PP, Zeier M, Schwenger V (2008) RAGE expression in the human peritoneal membrane. Nephrol Dial Transplant 23: 3302-6

11) Kitamura M, Nishino T, Obata Y, Furusu A, Hishikawa Y, Koji T, Kohno S (2012) Epigallocatechin gallate suppresses peritoneal fibrosis in mice. Chem Biol Interact 195:95-104

12) Hirose M, Nishino T, Obata Y, Nakazawa M, Nakazawa Y, Furusu A, Abe K, Miyazaki M, Koji T, Kohno S (2013) 22-Oxacalcitriol prevents progression of peritoneal fibrosis in a mouse model. Perit Dial Int 33:132-42

13) Volpi N (2011) Anti-inflammatory activity of chondroitin sulphate: new functions from an old natural macromolecule. Inflammopharmacology 19:299-306

14) du Souich P, Garcia AG, Verges J, Montell E (2009) Immunomodulatory and anti-inflammatory effects of chondroitin sulphate. J Cell Mol Med 13:1451-63

15) Baeza-Raja B, Muñoz-Cánoves P (2004) p38 MAPK-induced nuclear factor-kappaB activity is required for skeletal muscle differentiation: role of interleukin-6. Mol Biol Cell 15: 2013–2026

16) Omata T, Itokazu Y, Inoue N, Segawa Y (2000) Effects of chondroitin sulfate-C on articular cartilage destruction in murine collagen-induced arthritis. Arzneimittelforschung 50:148-53

17) Hori Y, Hoshino J, Yamazaki C, Sekiguchi T, Miyauchi S, Horie K (2001) Effects of chondroitin sulfate on colitis induced by dextran sulfate sodium in rats. Jpn J Pharmacol 85:155-60

18) Herrero-Beaumont G, Marcos ME, Sanchez-Pernaute O, Granados R, Ortega L, Montell E, Verges J, Egido J, Largo R (2008) Effect of chondroitin sulphate in a rabbit model of atherosclerosis aggravated by chronic arthritis. Br J Pharmacol 154:843-51

19) Obata Y, Nishino T, Kushibiki T, Tomoshige R, Xia Z, Miyazaki M, Abe K, Koji T,

Tabata Y, Kohno S (2012) HSP47 siRNA conjugated with cationized gelatin microspheres suppresses peritoneal fibrosis in mice. Acta Biomater 8:2688-96

20) Tan Y, Zhang JS, Huang L (2002) Codelivery of NF-kappaB decoy-related oligodeoxynucleotide improves LPD-mediated systemic gene transfer. Mol Ther 6:804-12.

21) Koji T, Komuta K, Nozawa M, Yamada S, Nakane PK (1994) Localization of cyclic adenosine 3',5'-monophosphate-responsive element (CRE)-binding proteins by southwestern histochemistry. J Histochem Cytochem 42:1399-405

22) Hishikawa Y, Damavandi E, Izumi S, Koji, T (2003) Molecular histochemical analysis of estrogen receptor alpha and beta expressions in the mouse ovary: in situ hybridization and southwestern histochemistry. Med Electron Microsc 36:67-73

23) Ashizawa M, Miyazaki M, Abe K, Furusu A, Isomoto H, Harada T, Ozono Y, Sakai H, Koji T, Kohno S (2003) Detection of nuclear factor-kappaB in IgA nephropathy using Southwestern histochemistry. Am J Kidney Dis 42:76-86

24) Lin CY, Chen WP, Fu LW, Yang LY, Huang PT (1997) Persistent transforming growth factor beta 1 expression may predict peritoneal fibrosis in CAPD patients with frequent peritonitis occurrence. Adv Perit Dial 13:64-71

25) Margetts PJ, Bonniaud P, Liu L, Hoff CM, Holmes CJ, West-Mays JA, Kelly MM

(2005) Transient overexpression of TGF-{beta}1 induces epithelial mesenchymal transition in the rodent peritoneum. J Am Soc Nephrol 16:425-436

26) Biswas SK, Mantovani A. (2010) Macrophage plasticity and interaction with lymphocyte subsets: cancer as a paradigm. Nat Immunol 11: 889-96

27)Yokoi H, Kasahara M, Mori K, Ogawa Y. Kuwabara T. Imamaki H, Kawanishi T, Koga K, Ishii A, Kato Y, Mori KP, Toda N, Ohno S, Muramatsu H, Muramatsu T, Sugawara A, Mukoyama M, Nakao K (2012) Pleiotrophin triggers inflammation and increased peritoneal permeability leading to peritoneal fibrosis. Kidney Int 81:160-9

28)Miyazaki M, Yuzawa Y (2005) The role of peritoneal fibrosis in encapsulating peritoneal sclerosis. Perit Dial Int 25:S48-56

29)Michel BA, Stucki G, Frey D, De Vathaire F, Vignon E, Bruehlmann P, Uebelhart D (2005) Chondroitins 4 and 6 sulfate in osteoarthritis of the knee: a randomized, controlled trial. Arthritis Rheum 52:779-86

30)Wildi LM, Raynauld JP, Martel-Pelletier J, Beaulieu A, Bessette L, Morin F, Abram F, Dorais M, Pelletier JP (2011) Chondroitin sulphate reduces both cartilage volume loss and bone marrow lesions in knee osteoarthritis patients starting as early as 6 months after initiation of therapy: a randomised, double-blind, placebo-controlled

pilot study using MRI. Ann Rheum Dis 70: 982-9

FIGURE LEGENDS

Figure 1—The result of Masson's trichrome staining of peritoneal tissues. (a) In the control group, injected with 15% ethanol dissolved in saline, the monolayer of mesothelial cells covered the entire surface of the peritoneum. (b) In the chondroitin sulfate (CS) group, peritoneal tissues were similar to that of the control group. (c) The peritoneal tissues of the mice in the chrolhexidine gluconate (CG) group showed marked thickening of the submesothelial compact zone and presence of numerous cells. (d) CS significantly suppressed the submesothelial thickening. (a–d), magnification 200×; bars indicate the thickness of the submesothelial compact zone. (e) Bar graph showing the thickness of the submesothelial compact zone. Data are expressed as mean ±standard error mean; * represents $p<0.05$.

Figure2－Immunohistochemistry for phosphorylated mitogen-activated protein kinase (p38MAPK) and extracellular signal-regulated kinase 1/2 (ERK1/2). (a) In the chrolhexidine gluconate (CG) group, a large number of phosphorylated p38MAPK-positive cells were present in the submesothelial compact zone. (b) Fewer phosphorylated p38MAPK-positive cells were observed in the CG + chondroitin sulfate (CS) group. (c) Bar graph showing the number of phosphorylated p38MAPK-positive cells. (d) In the CG group, the number of phosphorylated ERK1/2-positive cells was increased. (e) The number of phosphorylated ERK1/2–positive cells was reduced in the CG + CS group. (f) Bar graph showing the number of phosphorylated ERK1/2-positive cells. (a, b, d, and e), magnification 200×; bars indicate the thickness of the submesothelial compact zone. (c, and f) Bar graph showing the number of phosphorylated p38MAPK- and phosphorylated ERK1/2 -positive cells. Data are expressed as mean ±standard error mean; * represents $p<0.05$. (g; phosphorylated-p38MAPK, h; F4/80, and i; phosphorylated-ERK1/2) Almost all macrophages were positive for phosphorylated-P38MAPK and phosphorylated -ERK1/2. Arrow heads indicate positive cells.

Figure3－Detection of nuclear factor (NF)-κB by southwestern histochemistry (SWH) and immunohistochemistry for Ikappa B alpha (IκBα). The panels of SWH for activated NF-κB were evaluated using an image analyzer. The red color was assigned to positive cells. (a) In the chrolhexidine gluconate (CG) group, cells positive for activated NF-κB were detected in the submesothelial compact zone. (b, e) The number of cells positive for activated NF-κB was significantly lower in the CG + chondroitin sulfate (CS) group. (c, d) The sections were reacted with mutated NF-κB double-stranded oligo-DNA probe as negative control. (e) Bar graph showing the number of NF-κB-activated cells. Data are expressed as mean ± standard error mean; * represents $p<0.05$. (f) In the CG group, the number of IκBα-positive cells was small in the peritoneum. (g) Numerous IκBα-positive cells were observed in the CG+CS group. (a, b, c, d, f and g) magnification 200×; bars in the panels indicate the thickness of the submesothelial compact zone. (a, b, c, and d) Bars by the side of panels show that the same range of signal was colored in all panels. Arrow heads indicate positive cells.

Figure 4—Immunohistochemistry for monocyte chemoattractant protein-1 (MCP-1) and

interleukin-1beta (IL-1β), and enzyme-linked immunosorbent assay (ELISA) for MCP-1. (a) Cells expressing MCP-1 were present in thickened peritoneal tissues in the chrolhexidine gluconate (CG) group. (b) Compared with the CG group, the CG + chondroitin sulfate (CS) group showed a reduced number of MCP-1-positive cells. (c) Bar graph showing the number of MCP-1-positive cells. (d) Bar graph showing the concentration of MCP-1 in peritoneal effluent. The concentration of MCP-1 was significantly increased in the CG group compared with the control group. We observed significant reduction of the concentration of MCP-1 in the CG + CS group. (e) In the CG group, IL-1β positive cells were observed in the submesotherial compact zone. (f) Fewer IL-1β-positive cells were present in the CG + CS group. (g) Bar graph showing the number of IL-1β-positive cells (a, b, e, and f), magnification 200×; bars indicate the thickness of the submesothelial compact zone. (c, d, and g) Data are expressed as mean ± standard error mean; * represents $p<0.05$. Arrow heads indicate positive cells.

Figure 5—Immunohistochemistory for F4/80 and CD86. (a) In the chrolhexidine gluconate (CG) group, F4/80 positive macrophages were observed in the submesotherial compact zone. (b) Fewer macrophages were present the CG + chondroitin sulfate (CS)

group. (c) Bar graph showing the number of F4/80-positive macrophages. (d; CD86 and e; F4/80) almost all macrophages were positive for CD86 in the continuous sections of CG group. (a, b, d, and e), magnification 200×; bars indicate the thickness of the submesothelial compact zone. (c) Data are expressed as mean ± standard error mean; * represents $p<0.05$. Arrow heads indicate positive cells.

Figure 6―Immunohistochemistory for phosphorylated Smad2/3 and α-smooth muscle actin (α-SMA). (a) In the chrolhexidine gluconate (CG) group, a large number of phosphorylated Smad2/3-positive cells were observed. (b) Treatment with chondroitin sulfate (CS) markedly decreased the number of phosphorylated Smad2/3-positive cells. (c) Bar graph showing the number of phosphorylated Smad2/3-positive cells. (d) In the CG group, α-SMA expressing myofibroblasts were present in submesothelial compact zone. (e) In the CG + CS group, the numbers of α-SMA expressing myofibroblast was reduced. (f) Bar graph showing the number of α-SMA expressing myofibroblasts. (a, b, d, and e), magnification 200×; bars indicate the thickness of the submesothelial compact zone. (c, and f) Data are expressed as mean ± standard error mean; * represents $p<0.05$. Arrow heads indicate positive cells.

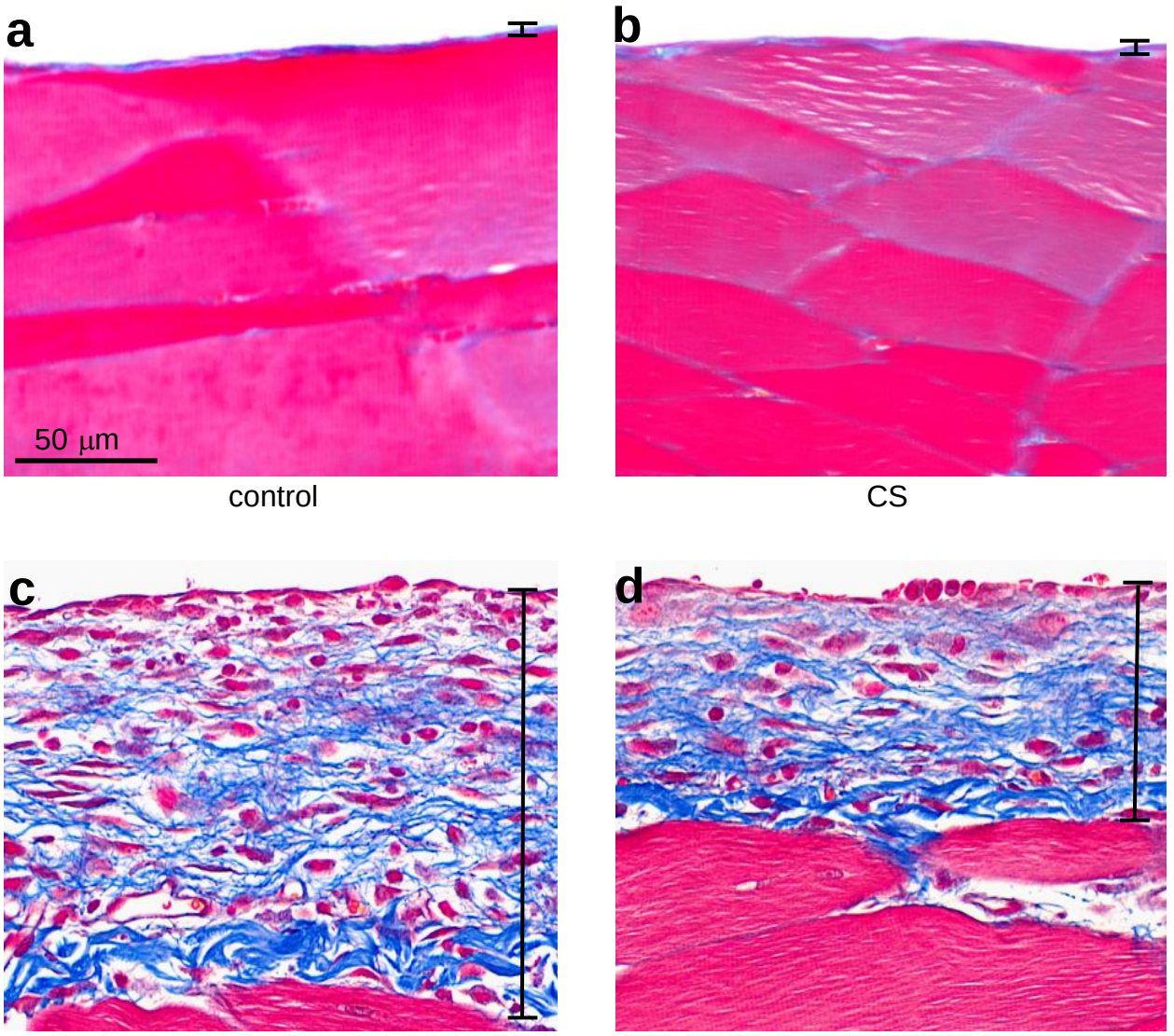
a
50 μm
control
b
CS
c
CG
d
CG+CS

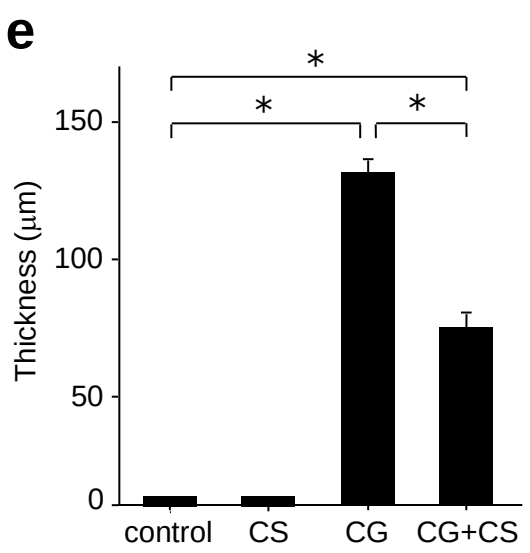
e
Thickness (μm)
150
100
50
0
*
*
*
control
CS
CG
CG+CS

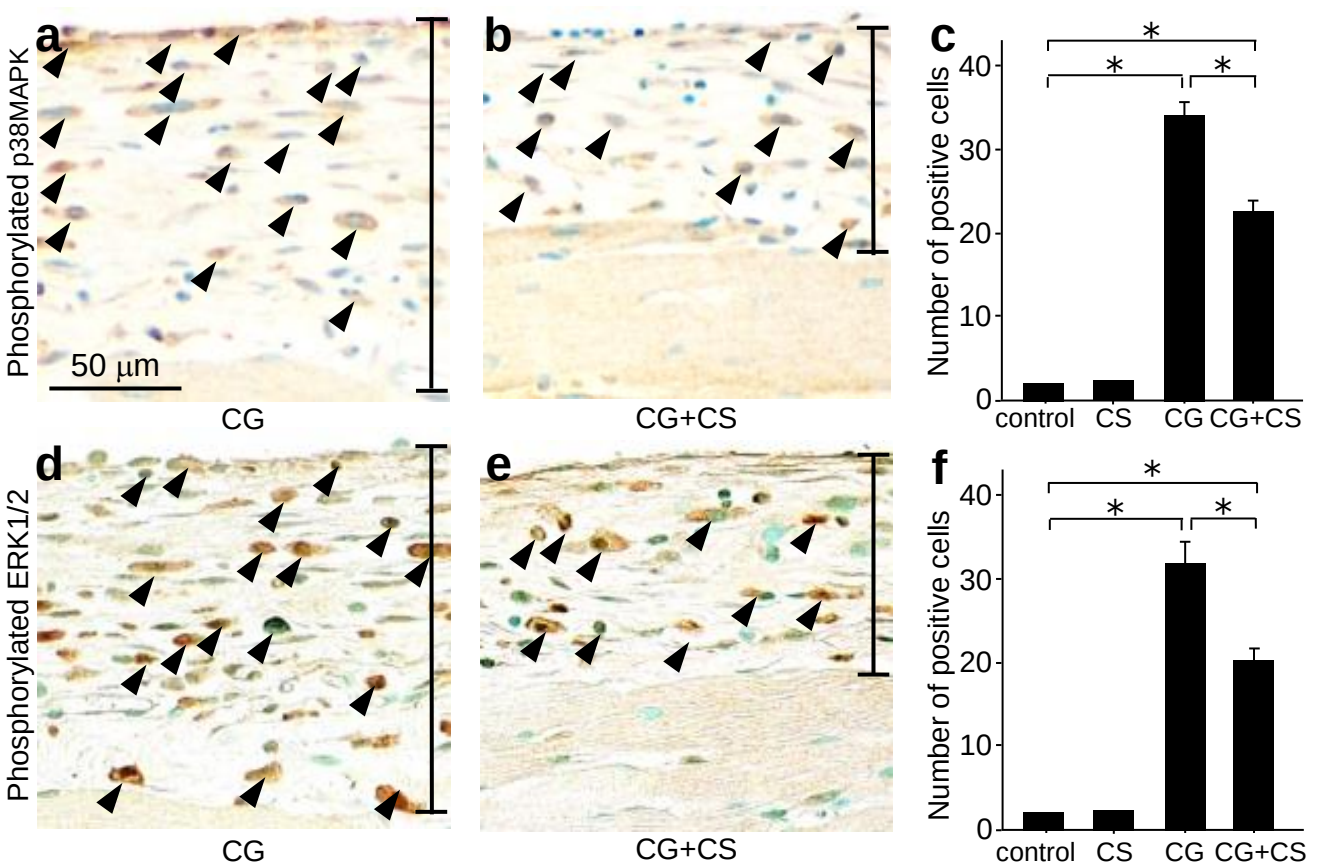
a
b
c
Phosphorylated p38MAPK
50 μm
CG
CG+CS
Number of positive cells
control
CS
CG
CG+CS
d
e
f
Phosphorylated ERK1/2
CG
CG+CS
Number of positive cells
control
CS
CG
CG+CS
g
h
i
Phosphorylated p38MAPK
F4/80
Phosphorylated ERK1/2

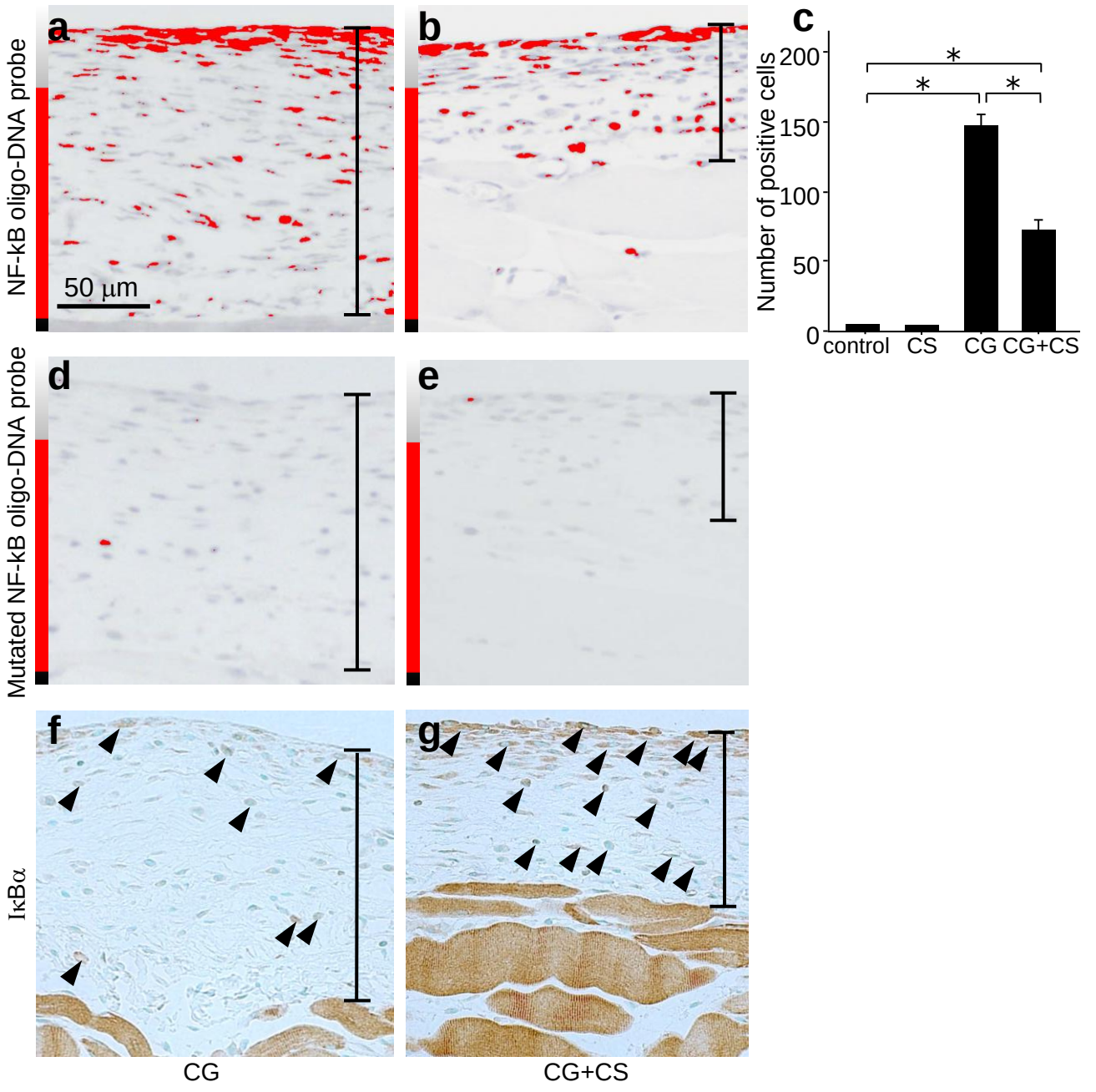
a
b
c
NF-kB oligo-DNA probe
50 μm
Number of positive cells
200
150
100
50
0
*
*
*
control
CS
CG
CG+CS
d
e
Mutated NF-kB oligo-DNA probe
f
g
IκBα
CG
CG+CS

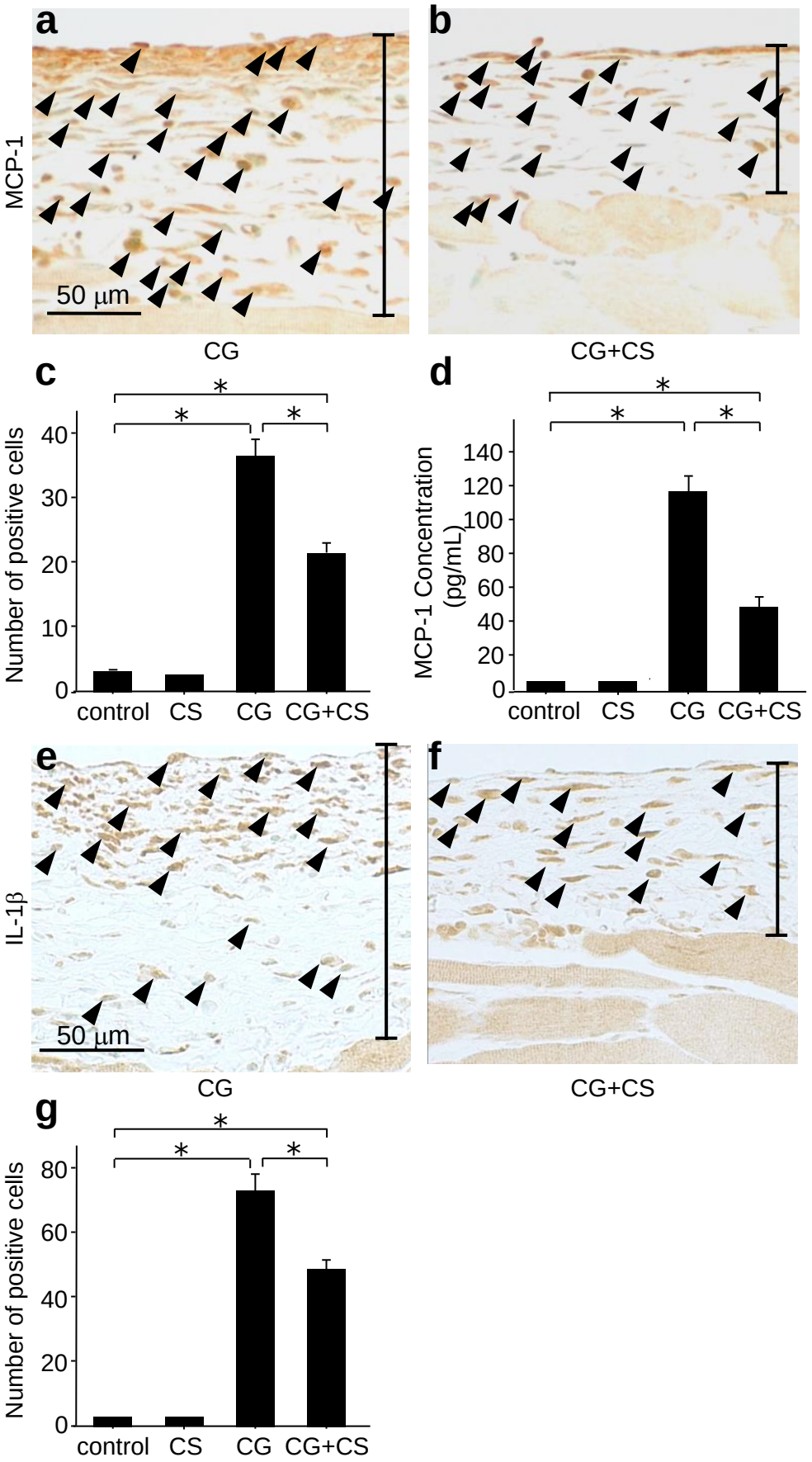
a
b
MCP-1
50 μm
CG
CG+CS
c
d
Number of positive cells
MCP-1 Concentration (pg/mL)
control
CS
CG
CG+CS
e
f
IL-1β
50 μm
CG
CG+CS
g
Number of positive cells
control
CS
CG
CG+CS

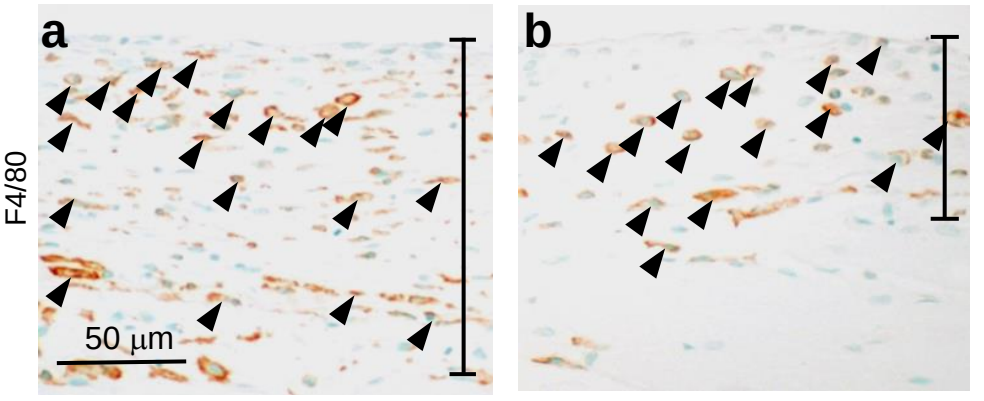
a
F4/80
50 μm
CG
b
CG+CS

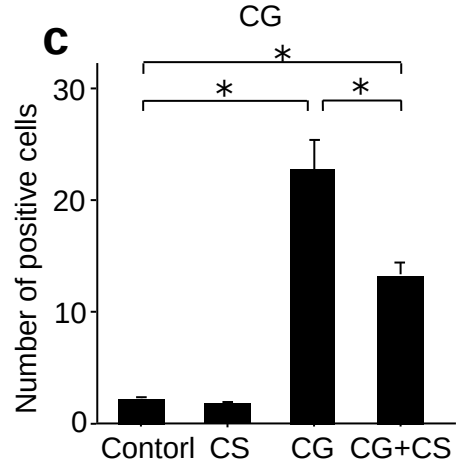
c
Number of positive cells
30
20
10
0
Contorl
CS
CG
CG+CS
*
*
*

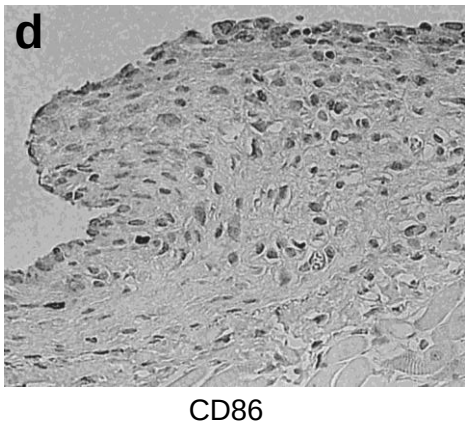
d
CD86

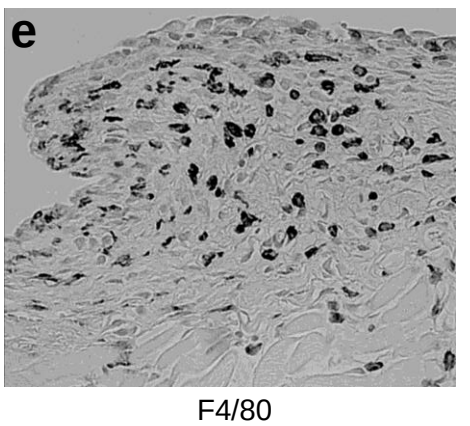
e
F4/80

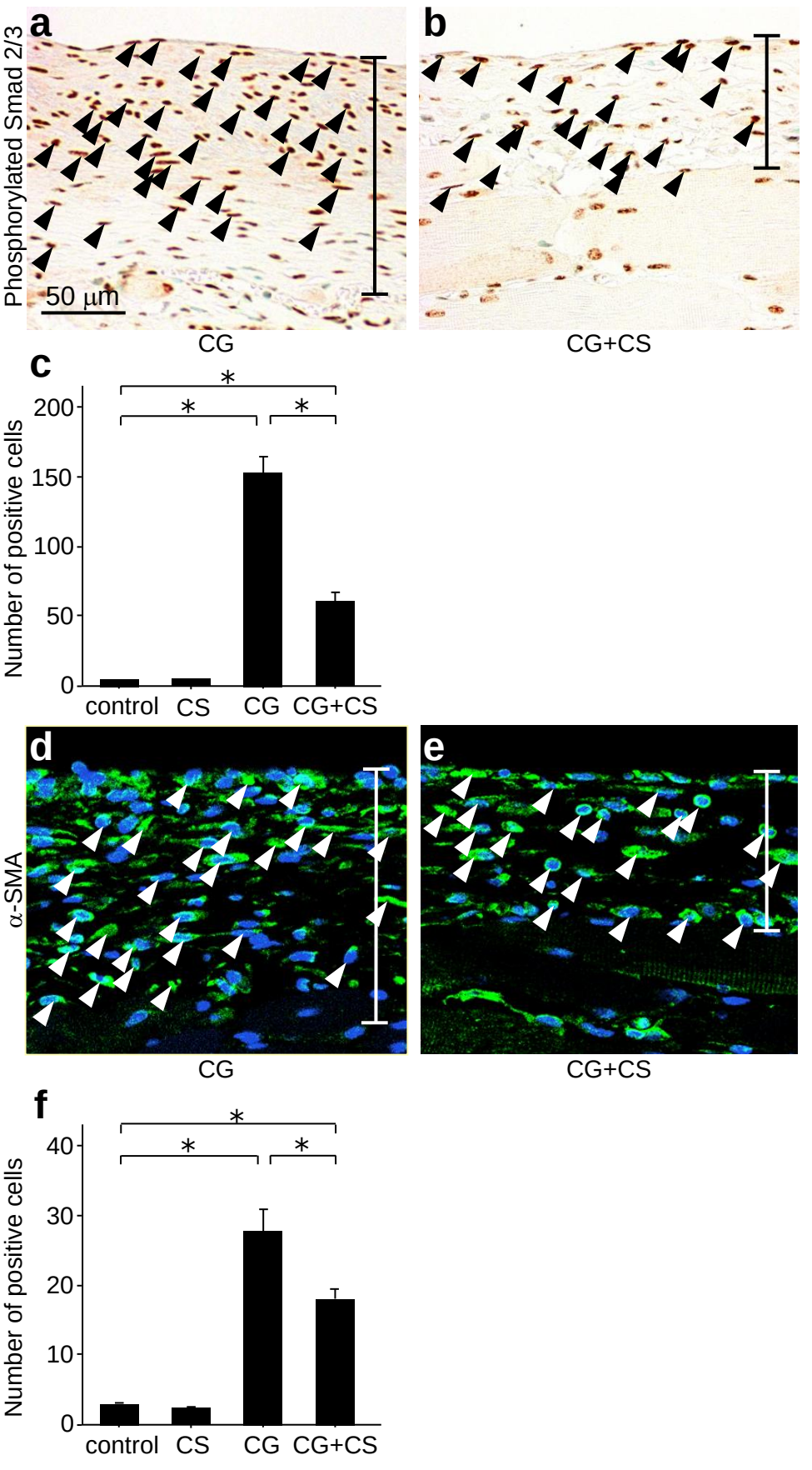
a
b
Phosphorylated Smad 2/3
50 μm
CG
CG+CS
c
Number of positive cells
200
150
100
50
0
control
CS
CG
CG+CS
d
e
α-SMA
CG
CG+CS
f
Number of positive cells
40
30
20
10
0
control
CS
CG
CG+CS